Energy 45 (2012) 840–849

Contents lists available at SciVerse ScienceDirect

Energy

journal homepage: www.elsevier.com/locate/energy

Reverse gas-lift technology for CO_2 storage into deep saline aquifers

Mohammad Javad Shafaei, Jalal Abedi*, Hassan Hassanzadeh, Zhangxin Chen

Department of Chemical & Petroleum Engineering, Schulich School of Engineering, University of Calgary, 2500 University Drive NW, Calgary, AB, Canada T2N 1N4

ARTICLE INFO

Article history:
Received 18 January 2012
Received in revised form
4 June 2012
Accepted 3 July 2012
Available online 9 August 2012

Keywords:
CO_2 storage and sequestration
Deep saline aquifer
Compression cost
Injection well
Gas-lift

ABSTRACT

We have developed an injection well design to reduce the cost of CO_2 sequestration. In this design, we propose a reverse gas-lift technology for simultaneous injection of CO_2 and water into aquifers. Saline water, which is produced at a location distant from the storage site, is pumped into a well through tubing; CO_2 is injected using the annular space between the tubing and the casing. One way gas-lift valves installed along the tubing allow the flow of CO_2 from the annulus into the tubing. This design makes the injection achievable at lower wellhead pressures, thereby, decreasing the compression costs. Simulation results demonstrate that the compression cost is lower than when a conventional injection scheme is used. The results also reveal that the proposed design can decrease the energy consumption for CO_2 sequestration. These results have implications for the large-scale implementation of CO_2 sequestration.

1. Introduction

The rising trend in the Earth's average temperature and its consequences in climate changes are concerns of the public and governments all around the world. It is believed that anthropogenic greenhouse gases are responsible for most of the observed temperature increase since the middle of the twentieth century. Carbon dioxide (CO_2) emissions from the use of fossil fuels form a significant portion of these gases [1,2].

One of the most promising proposed mitigations for reducing CO_2 emissions is CO_2 capture and sequestration (CCS) [1–3]. CCS is a process that consists of separation of CO_2 from industrial and energy-related sources, compression, transportation to a storage location, and long-term isolation from the atmosphere [4]. The geological sequestration of CO_2 can be accomplished in depleted oil and gas reservoirs, coal seams, and deep saline aquifers. The potential storage capacities of these candidates are different, with the highest capacity related to deep saline aquifers [5,6]. The high potential of deep saline aquifers has encouraged scientists to study this option since the early 1990s.

Several mechanisms can lead to permanent storage of CO_2 in deep saline aquifers, including solubility trapping [6,7], residual phase trapping [8–10], and mineral trapping [11–13]. In early studies, van der Meer [14] recognized that aquifers' pore pressure increases with CO_2 injection in compartmentalized or low-permeability reservoirs, which can potentially decrease the capacity of storage. Ghaderi et al. [15] demonstrated that the injection of large volumes of CO_2 within a relatively small area and a short period of time limits the injection capacity. It has been concluded, therefore, that the injection of a substantial amount of CO_2 in a saline aquifer may be a very difficult task. The injection capacity may be much lower than the estimated pore space for storage, because the reservoir pressure during injection may quickly exceed the fracture pressure; therefore, injection is stopped before a target amount is injected.

Moreover, after injecting CO_2 into an aquifer, the injected mobile supercritical phase migrates upward and spreads under the sealing rock, due to its buoyancy. When CO_2 is in the free mobile phase, there is always a risk of leakage through natural and artificial pathways [16]. Once CO_2 is dissolved into brine, it cannot migrate upwards other than by diffusion and can then be maintained with a negligible risk of leakage.

Some studies have been done using reservoir engineering techniques to accelerate the CO_2 dissolution rate. In such methods, the formation brine can be produced at a distant location and pumped back on the top of the injected CO_2 plume. Hassanzadeh et al. [17] and Keith et al. [18] investigated the role of brine injection on the top of a CO_2 plume in accelerating CO_2 dissolution in formation brines.

In an extension to their work, Hassanzadeh et al. [19] used a black oil reservoir simulation approach to perform more comprehensive numerical simulations for investigating the role of brine injection on the top of a CO_2 plume, leading to accelerated

* Corresponding author.
E-mail address: jabedi@ucalgary.ca (J. Abedi).

0360-5442/$ – see front matter © 2012 Elsevier Ltd. All rights reserved.
http://dx.doi.org/10.1016/j.energy.2012.07.007

solubility trapping mechanisms. In a traditional black oil reservoir simulator the liquid hydrocarbon phase is treated as if it has only two components —oil and gas— with a simple, pressure-dependent solubility law of the gas in the liquid phase. Using such an approach one can simulate a CO_2-water system by replacing gas by CO_2 and oil by water. A detailed treatment of the CO_2-brine system using a black oil flow simulator has been reported elsewhere [18]. The authors proposed an engineering design for accelerating CO_2 dissolution and showed a potential acceleration using simultaneous brine and CO_2 injection. They concluded that, in comparison with CO_2 capture and compression costs, brine pumping may be cost-effective in terms of energy expenses.

Surface mixing of CO_2 and brine has also been reported in the literature [20,21]. The disadvantage of this scenario may be in the capital and operational costs of the surface processing facilities for water and CO_2 mixing.

In this paper, we propose a new well string design for simultaneous injection of CO_2 and brine to decrease the required pumping and compression power associated with CO_2 disposal. In the following section, a description of the system is presented, followed by the model development, results and discussion, and a brief conclusion.

2. System description

In this study, a new design is presented for the injection of CO_2. This proposed design decreases the required power associated with the sequestration of CO_2 in deep saline aquifers. In this work, a tubing well string configuration equipped with gas-lift valves is proposed for simultaneous injection of CO_2 and brine into the saline aquifers.

Fig. 1 depicts the arrangement of the proposed well string used for simultaneous injection of CO_2 and water. This system consists of a gas compression station, a water pump and a tubing string with installed gas-lift valves. The space between the wellbore casing and tubing is called annulus. Water and CO_2 are injected into the tubing and annulus, respectively. Gas-lift valves provide communication between the annulus and tubing. The gas-lift valves with preset opening and closing pressures situated in the gas-lift mandrel are used to control and maintain flow of the injected CO_2 from the annular space into the tubing. The gas-lift valves (similar to those used in the petroleum industry for gas-lift operations for oil production) in the mandrel allow the injection of CO_2 into the tubing. A detailed description of the gas-lift valves is given by Guo et al. [22].

The introduction of CO_2 from the annulus into the tubing through gas-lift valves causes mass transfer between CO_2 and brine, thereby increasing the dissolution of the CO_2 into the water. Such a dissolution process can be conducted at the surface. However, this new design is more efficient, since we benefit from higher solubility of CO_2 in brine and higher pressure provided from the well column compared to the surface condition. In addition, the proposed design leads to a decrease in the cost associated with CO_2 compression and water pumping.

The development of a model for the investigation and simulation of the behavior of such a system for CO_2 storage applications is the main goal of the next section.

3. Model development

To develop a model for the proposed process, the whole configuration is first considered as a combination of links, sources, sink and junction nodes, as shown in Fig. 2. The CO_2 and water feed points are source nodes, the point of the injection into the aquifer is called a sink node, and each of the upstream and downstream valve points is considered a junction node. The process parameters that should be determined at each node are the pressure and flow rate. The aim is the computation of the unknown variables at these nodes.

As mentioned above, two sources exist in the proposed configuration. The nodes of the annulus line and tubing line are source points (AP_1 and TP_1, respectively) in which the injected CO_2 and water flow rates are given. Pressures at these points are unknown and should be calculated. There is just one sink node in the tubing (TP_N). Since the mixture of CO_2 and water should be injected into a saline aquifer, the well bottomhole pressure is dependent on the saline aquifer pressure and, therefore, should be greater than the saline aquifer pressure. In this study, it is assumed that injection into the saline aquifer happens at a constant bottomhole pressure. This assumption can be justified by balancing the volume of injected water produced from and injected into the saline aquifer as shown in Fig. 1. Therefore, the well bottomhole pressure at the tubing line (sink node) is a known parameter.

Fig. 2 shows the detailed network configuration in the proposed design. Each point upstream and downstream of the gas-lift valves (injection points) is considered a node (AP_i and TP_i, respectively). The number of nodes is dependent on the number of injection points or gas-lift valves. The connection between these nodes is provided by links. In the proposed design three types of links are considered including: the link between the annulus and tubing

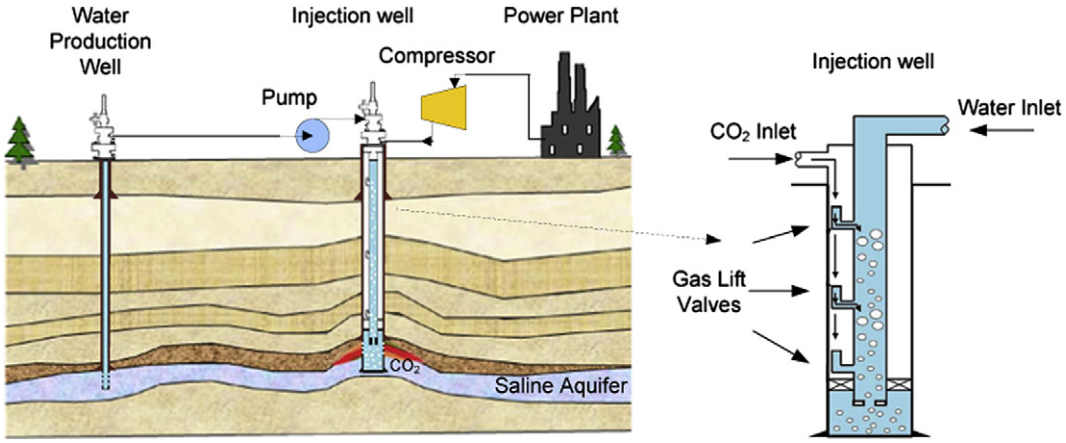

Fig. 1. Configuration of the proposed well string used for simultaneous CO_2 and water injection.

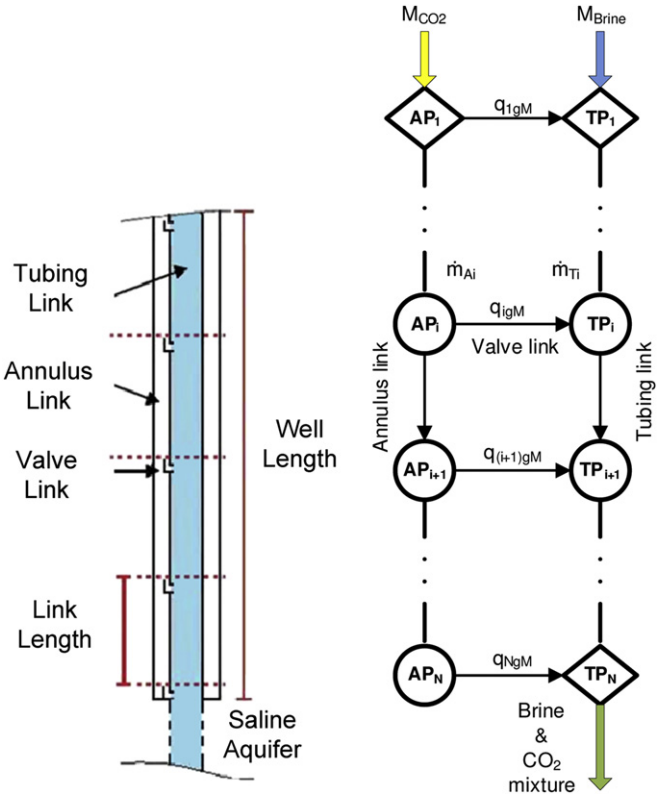

Fig. 2. Schematic of the network configuration.

through the gas-lift valves (CO_2 flow through the valves), the annulus links (vertically downward CO_2 fluid flow through the annulus), and the tubing links (vertically downward CO_2-water fluid flow through the tubing). The required equations to calculate the unknown parameters should be defined. The fluid flow equations for all gas-lift valve, tubing and annulus links shown in the network configuration should be included to complete the model. These equations for different sections are coupled together and need to be solved simultaneously. Based on the inlet condition at the top of the well and the aquifer pressure all the required parameters can be obtained.

In the following subsections, the modeling of the valve, annulus and tubing sections are presented, and a method for solving the coupled system is then described.

3.1. Modeling of the valves

The injected mass flow rate through the valves can be determined by a choke flow equation [22]. The pressures upstream and downstream of the injection choke are the annulus and tubing pressures at the corresponding nodes, respectively. There is no universal equation for calculation of the mass flow rate through a choke for all types of production fluids. Different choke models are available in the literature for single-phase and multi-phase flows; the choke model must be chosen based on the flow regime, i.e., subsonic or sonic flow. If the fluid velocity in the choke throat exceeds the sound velocity at in situ conditions, the flow regime is sonic. Fluid velocities less than the sonic flow conditions are considered to be subsonic.

At sonic flow conditions, variations in the downstream pressure do not affect the upstream pressure. The existence of sonic flow through a choke depends on the downstream to upstream pressure ratio. If this pressure ratio is less than the critical pressure ratio, the flow regime is sonic. On the other hand, if the ratio is equal to and greater than the critical pressure ratio, it is called subsonic. Gas-lift valves are considered one way; therefore, when the casing pressure is less than the tubing pressure, the valves do not operate and there is no flow rate through the valves.

The process in the choke is assumed to be isentropic, since it is adiabatic (no time for heat transfer); the friction loss is assumed to be negligible at the choke. We use the following equations to calculate the CO_2 flow rate through the valve for sonic and subsonic flow regimes [22]:

$$\text{Sonic flow}: \quad q_{gM} = 4.17\times10^{6}C_cA_cP_{up}\sqrt{\left(\frac{k}{\gamma_g T_{up}}\right)\left(\frac{2}{k+1}\right)^{\frac{k+1}{k-1}}} \tag{1}$$

$$\text{Subsonic flow}: \quad q_{gM} = 6.09\times10^{6}C_cA_cP_{up}\sqrt{\left(\frac{k}{(k-1)\gamma_g T_{up}}\right)\left[\left(\frac{P_{dn}}{P_{up}}\right)^{\frac{2}{k}}-\left(\frac{P_{dn}}{P_{up}}\right)^{\frac{k+1}{k}}\right]} \tag{2}$$

where q_{gM} is the gas flow rate in Msm^3/day, P_{up} is the upstream pressure of the choke (casing node pressure) in MPa, A_c is the choke cross-sectional area in m^2, T_{up} is the upstream temperature of the choke (casing node temperature) in degrees Kelvin, γ_g is the gas specific gravity, and C_c is the choke flow coefficient.

The following correlation gives the choke flow coefficient with reasonable accuracy for a Reynolds number between 10^4 and 10^6 [23]:

$$C_c = \frac{d_c}{D}+\frac{0.3167}{(d_c/D)^{0.6}}+0.025[\log N_{Re}-4] \tag{3}$$

where N_{Re} is the Reynolds number, d_c is the choke diameter in meter, D is the pipe diameter in meter, and μ is the gas viscosity at in situ pressure and temperature in mPa-sec. Beyond a Reynolds number of 2×10^6, the choke flow coefficient remains constant. For the proposed design the Reynolds number is within 7×10^5 and 8×10^6 and, therefore, this correlation can be used. Since the Reynolds number and, consequently, the choke flow coefficient (C_c) are dependent on the gas flow rate, a trial-and-error method is used to calculate the gas flow rate.

3.2. Modeling of the annulus and tubing links

It was previously mentioned that, depending on the number of injection points, the annulus and tubing sections are divided into several links. Each link starts from a source/junction node and ends at a junction/sink node. The first parameter that is important in our calculations is the input amount of CO_2 into the annulus link (i.e.,$\dot{m}_{A1}$ at the injection point "i" for the annulus link). This amount is dependent on the CO_2 injected through the valves at upper injection points. Therefore, it can be calculated for each annulus link using the following equation:

$$\dot{m}_{Ai} = M_{CO_2}-\sum_{j=1}^{i}\rho_{gS}q_{gMj} \tag{4}$$

where $\dot{m}_{Ai}$ is the input mass flow rate of CO_2 into the annulus link in kg/sec, M_{CO_2} is the total injected CO_2 into the well in kg/sec, ρ_{gs} is the CO_2 density in kg/m^3 at standard conditions, and q_{gMj} is the injected CO_2 through valve "j" in standard m^3/sec.

The total amount of the injected CO_2 and water at the beginning of the tubing link can be easily calculated. Since the water is just fed into the tubing line, the total amount of the injected water at the beginning of every tubing link is equal to M_{water}, as shown in Fig. 2. Moreover, the mass of the injected CO_2 is the sum of the injected CO_2 through the upper valves, which is shown in the following equation:

$$\dot{m}_{Ti} = \sum_{j=1}^{i} \rho_{gS} q_{gMj} \tag{5}$$

where $\dot{m}_{Ti}$ is the input mass flow rate of CO_2 into the tubing link in kg/sec, ρ_{gs} is the CO_2 density in kg/m^3 at standard conditions, and q_{gMj} is the injected CO_2 through valve "j" in standard m^3/sec.

Another parameter in the calculation is the flowing wellbore temperature profile. From the reported modeling data, the fluid temperature along the well can be approximated by a linear function of the depth along the well, as given by $T(z) = T_s + Gz$, where $T(z)$ is the fluid temperature at the depth equal to z in °C, T_s is the surface temperature in °C, G is the temperature gradient in °C/m, and z is the depth in m [24].

To determine the pressure drop (dp) along tubing and annulus links, we discretize each link to a number of segments (dL). A step-by-step procedure is used to solve the segment calculations [25]. This procedure is called a marching algorithm, which is outlined in Fig. 3. Detailed equations for pressure drop calculations are given by Beggs and Brill [25]. The calculation procedure starts from a given point such as an input/outlet node with a predetermined

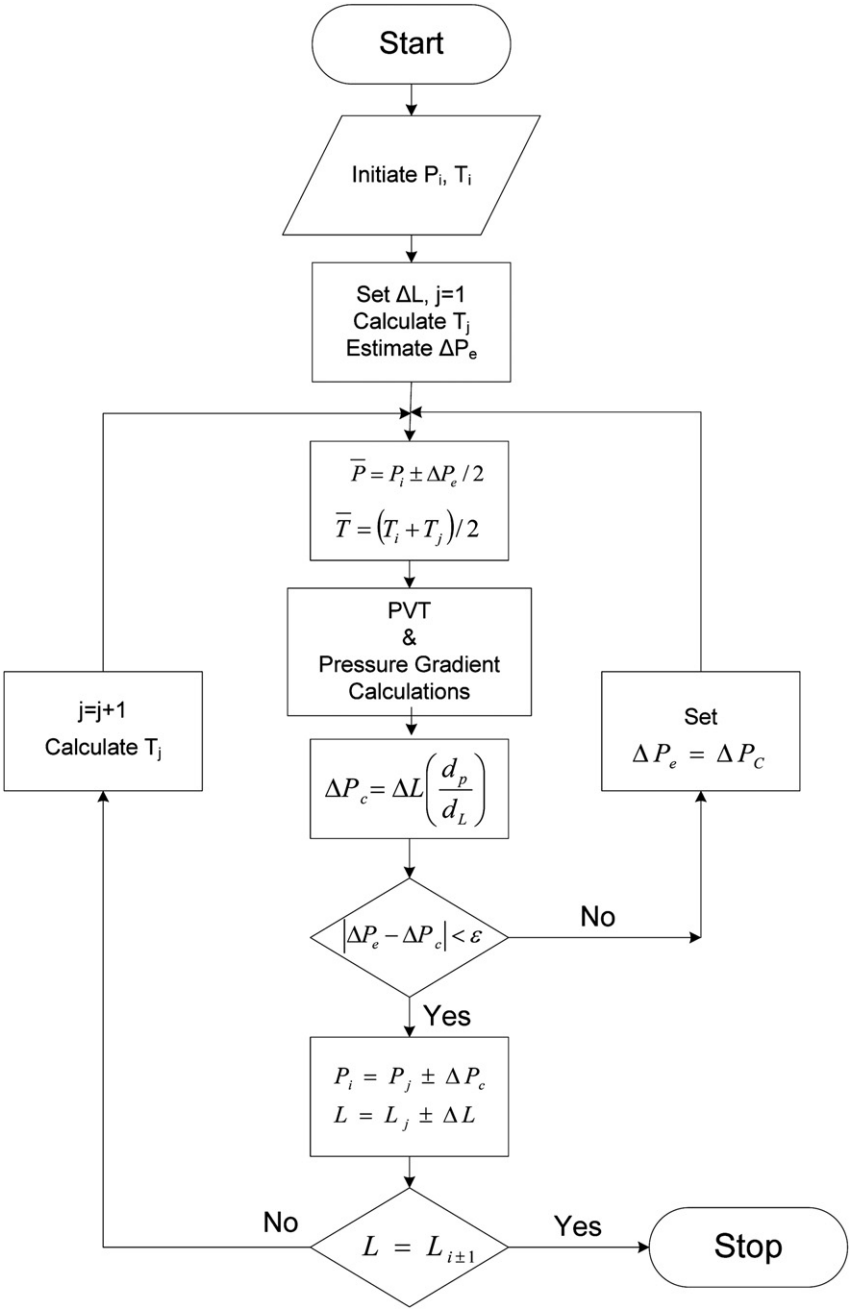

Fig. 3. Flow chart of the single-link calculation procedure.

segment length, pressure and temperature. Thus the input mass ($\dot{m}_{Ai}$, $\dot{m}_{Ti}$) and temperature $T(z)$ can be determined. After determining the average pressure and temperature along the segment, a CO_2-brine PVT (pressure, volume, temperature) program[1] is used for the determination of CO_2 and brine PVT properties [25]. The pressure drop calculation along the segment, ΔPe, is then performed using Beggs and Brill's method [26].

These calculations are conducted in an iterative manner, as shown in Fig. 3. The procedure described in this figure returns the calculated pressure difference between two subsequent nodes for tubing and annulus links and are denoted as ΔAP_i and ΔTP_i for the annulus and tubing links, respectively.

The overall pressure gradient consists of three terms [27]. The first term is called the acceleration term, the effect of which on the total pressure gradient is negligible as compared to other forms of the pressure drop, because there is no change in the diameter for the links or segments and the CO_2 density variation in the annular space is not significant. The other two terms are the static and friction loss pressure terms. The fluid flow regime through the annulus link is vertically downward and a single-phase; therefore, static and friction pressure loss can be simply calculated using CO_2 properties and velocity. The friction factor is a function of the flow regime that is determined by the Reynolds number and the relative roughness of the tubing. Chen's equation, which approximates the Moody friction factor, is used to calculate the single-phase friction factor [28].

Although the same procedure is applied for the pressure distribution through the tubing link, the segment pressure gradient is much more complicated in the tubing. The complexity arises because the fluid flow is two-phase and CO_2 dissolution occurs along the tubing link.

3.3. Pressure drop calculation in the tubing link

As described in the previous section, the injected CO_2 from the annulus contacts the injected water in the tubing. Since the water is undersaturated with respect to CO_2, a fraction of the CO_2 dissolves into the water. In addition, the injected CO_2 is also undersaturated (dry) with respect to water vapor; therefore, a fraction of the aqueous phase evaporates into the gaseous phase. These dissolution and evaporation processes occur in the tubing links, resulting in variations of the flow rate of the gaseous and aqueous phases. Due to the evaporation of the water, the liquid flow rate slightly decreases across the link. If it is assumed that the CO_2 phase is saturated by water, the liquid flow rate can be easily computed by subtracting the evaporated water from the total injected brine flow rate at the beginning of the segment.

The mutual solubility for the water-CO_2 system at the prevailing conditions are found by a procedure described by Hassanzadeh et al. [26]. The dissolved CO_2 in water can be represented by the solution gas-water ratio, R_S, which is the standard volume of CO_2 dissolved in water per unit volume of water at standard conditions. In addition, the water volume at the prevailing pressure and temperature increases due to the dissolution of CO_2 in the water. The relative change in the volume of CO_2 saturated brine to its standard volume is represented by the formation volume factor, which is denoted by B_w. Taking into account dissolution and evaporation processes, the gas and liquid flow rates can be determined using the following equations:

$$Q_L = (Q_w - W_c Q_G) B_w \tag{6.1}$$

$$Q_G = (Q_{CO_2} - R_s Q_w) B_g \tag{6.2}$$

where Q_L is the liquid flow rate in m^3/sec, Q_G is the gas flow rate in m^3/sec, Q_w is the inlet water flow rate in standard m^3/sec, Q_{CO_2} is the inlet CO_2 flow rate in standard m^3/sec, W_c is the water content of CO_2 in m^3/standard m^3 of CO_2, B_w is the water formation volume factor in m^3/standard m^3, B_g is the CO_2 formation volume factor in m^3/standard m^3, and R_s is the solution gas-water ratio. In Equations (6.1) and (6.2), the second terms contribute to evaporation of water and dissolution of CO_2 in water, respectively.

The CO_2 concentration in water can be obtained using the following equation:

$$C_{CO_2} = \frac{R_s \rho_{gs}}{B_w} \tag{7}$$

This formulation leads to the maximum expected dissolution, which is the equilibrium concentration of CO_2 in brine and is about 2.5 mole percent. In practice, the injected CO_2 and water may not reach equilibrium, and other means of enhancing mass transfer between the two phases may be necessary. However, since the dissolution of CO_2 into brine is very small (about 2.5 mole percent), the pressure distribution and concentration profile can be decoupled from the phase equilibrium or PVT data.

3.4. Integrated model

The development of the model for injecting CO_2 and water through the proposed well string configuration is based on the integration of the sink, source and junction nodes. CO_2 and water feed points are the source nodes and aquifer sinks, and each of upstream/downstream valves are considered as the junction nodes.

The process parameters that should be determined at each node are the pressure and flow rate. Due to the dependence of all nodes on each other through the links, the whole system must be solved simultaneously. Therefore, an integrated model to solve the whole system is presented in this subsection.

Since all the described nodes are connected together with links, these links relate the node process parameters and should be modeled properly. Thus far, the choke, annulus and tubing sections have been modeled. Therefore, after determining the model for each section, the known and unknown variables are defined, and the integrated system of equations then needs to be established. Finally, this system of equations is solved to find the unknown parameters. This procedure is described in more detail in the following paragraphs.

For an integrated system with N valves, the total number of nodes is 2N and there are 4N process variables (the pressure and flow rate of 2N nodes). Three process variables are the known parameters, including the mass flow rates of the total injected brine and CO_2 and the bottom well tubing pressure, which is dependent on the aquifer pressure. Therefore, 4N-3 independent equations should be determined to completely define a system of equations for finding the unknown variables. The number of equations can be further reduced by using the continuity equations for N-1 links in the annulus and tubing lines, as represented by Equations (4) and (5), resulting in a reduction of 2N-2 equations. Consequently, the number of equations is reduced to 4N-3-(2N-2) = 2N-1. Therefore, the actual unknown variables are all node pressures, except the last tubing node pressure (TP_N), which is the aquifer pressure.

Since there are 2N-1 unknown pressures, 2N-1 independent equations are required. For link "i" in the annulus and tubing lines, the following equations can be written, respectively:

$$AP_i - AP_{i+1} = \Delta AP_i(TP_1, \ldots, AP_1, \ldots) \tag{8.1}$$

$$TP_i - TP_{i+1} = \Delta TP_i(TP_1, \ldots, AP_1, \ldots) \tag{8.2}$$

[1] This computer program is available up on request from. hhassanz@ucalgary.ca.

where AP_i is the annulus pressure at injection valve "i" in Pa, AP_i is the tubing pressure at injection valve "i" in Pa, and ΔAP_i and ΔTP_i are the pressure drops for the annulus and tubing sections, respectively.

All the variables in the system are independent variables in these functions. Thus far, 2N-2 equations have been determined. The last equation is the mass balance equation over the injected mass flow rate of CO_2 to the system and the sum of the injected CO_2 through all valves:

$$M_{CO_2} = \sum_{j=1}^{N} \rho_{gS} q_{gMj} \tag{9}$$

where M_{CO_2} is the total injected CO_2 into the system in kg/sec, ρ_{gs} is the CO_2 density at standard conditions in kg/m^3, and qgMj is the injected CO_2 through valve "j" in standard m^3/sec.

Writing Equations (8.1) and (8.2) for all nodes and Equation (9) for node N-1, we reach a system of nonlinear equations as given by:

$$\begin{cases} F_1(TP_1,\ldots,AP_1,\ldots)=TP_1-TP_2-\Delta TP_1(TP_1,\ldots,AP_1,\ldots)=0 \\ \vdots \\ F_{N-1}(TP_1,\ldots,AP_1,\ldots)=TP_{N-1}-TP_N-\Delta TP_{N-1}(TP_1,\ldots,AP_1,\ldots)=0 \\ F_N(TP_1,\ldots,AP_1,\ldots)=AP_1-AP_2-\Delta AP_1(TP_1,\ldots,AP_1,\ldots)=0 \\ \vdots \\ F_{2N-2}(TP_1,\ldots,AP_1,\ldots)=AP_{N-1}-AP_N-\Delta AP_{N-1}(TP_1,\ldots,AP_1,\ldots)=0 \\ F_{2N-1}(TP_1,\ldots,AP_1,\ldots)=M_{CO_2}-\sum_{j=1}^{N}\rho_{gS}q_{gMj}=0 \end{cases} \tag{10}$$

where $F_i(TP_1, \ldots, AP_1,\ldots)$ represents the residual of the pressure drop for node "i", which is a function of all the variables in the system. This residual can be evaluated using Beggs and Brill's procedure [25]. To evaluate this function at each node, parameters such as the mass flow rate of the injected CO_2 and water described in Equations (4)–(6), the tubing and annulus diameters and the physical properties of CO_2 and water are needed.

The Newton–Raphson method is used to solve the above nonlinear system of equations [29]. Due to the nonlinearity of the system of equations and the discontinuity in the choke equations (which leads to a high possibility of independence of the annulus and tubing line pressures), very accurate initial guesses are needed; otherwise, the system diverges. After determining the initial guesses for the unknown pressures, the following equations are used to gradually improve the convergence and, consequently, approach the converged solution for the system of nonlinear equations.

$$\begin{bmatrix} \frac{\partial F_1}{\partial TP_1} & \cdots & \frac{\partial F_1}{\partial TP_{N-1}} & \frac{\partial F_1}{\partial AP_1} & \cdots & \frac{\partial F_1}{\partial AP_N} \\ \vdots & & \vdots & \vdots & & \vdots \\ \frac{\partial F_{2N-1}}{\partial TP_1} & \cdots & \frac{\partial F_{2N-1}}{\partial TP_{N-1}} & \frac{\partial F_{2N-1}}{\partial AP_1} & \cdots & \frac{\partial F_{2N-1}}{\partial AP_N} \end{bmatrix}^k \begin{bmatrix} \delta(TP_1) \\ \vdots \\ \delta(TP_{N-1}) \\ \delta(AP_1) \\ \vdots \\ \delta(AP_N) \end{bmatrix}^{k+1} = \begin{bmatrix} F_1 \\ \vdots \\ F_{N-1} \\ F_N \\ \vdots \\ F_{2N-1} \end{bmatrix}^k \tag{11}$$

The first matrix is a coefficient matrix, which is the Jacobian matrix of 2N-1 functions (F_1, …, F_{2N-1}) with respect to 2N-1 variables (TP_1,…, TP_{N-1}, AP_1,…, AP_N) for k iterations to find the final solution. The right-hand side vector, F, represents the residuals of the functions for iteration k. The second column vector, δ, on the left-hand side of the equation is the correction matrix, which is calculated by multiplying the inverse of the Jacobian matrix by the residual matrix. The unknown values are updated, and the iteration continues until a final solution of the system with acceptable accuracy is obtained. In all simulations a pressure difference of 10 kPa (1.45 psi) was used as a convergence limit.

4. Results and discussion

4.1. Integrated model simulations

In this section, the simulation of a complete well string configuration that injects CO_2 and water into a saline aquifer is discussed. First, a sensitivity analysis to the flowing temperature gradient is presented. A mass flow rate of 30,000 kg/hr (~0.26 Mt/yr) brine was injected into tubing with an internal diameter of 10 cm, and CO_2 was injected at 20,000 kg/hr (~0.17Mt/year) into a saline aquifer at a depth of 1000 m. The internal diameter of the casing was 14 cm. A gas-lift valve, with a diameter of 2.54 cm (1 in.), was placed just below the wellhead, and the CO_2-brine mixture was injected into the saline aquifer at 7 MPa (~1000 psia). Simulations were conducted for three flowing temperature gradients along the tubing: 0.01, 0.02 and 0.03 °C/m.

The concentration profiles for different cases were calculated, and those along the tubing section are shown in Fig. 4. The results show that the higher temperature gradient along the tubing results in lower dissolution of CO_2 into brine. Fig. 4 also shows that, for the lower temperature gradient along the tubing, the CO_2 concentration had an increasing trend because, in this case, the pressure was the dominant factor and dissolution was an increasing function of pressure. On the other hand, for the higher temperature gradient (0.03 °C/m), the CO_2 concentration decreased with depth, demonstrating that temperature was the predominant factor, due to the CO_2 dissolution decreasing with increasing temperature. In addition, Fig. 4 shows that, for the problem studied here, a flowing temperature gradient of 0.02 °C/m was close to the turning point between the increasing and decreasing trends of dissolution.

Fig. 5 shows pressure profiles along the tubing and annulus sections. Although the concentration profiles were different among three cases, as shown in Fig. 4, there was no significant difference between the tubing pressures of these three cases, primarily because the CO_2 dissolution was small and did not have a significant effect on the liquid hold up along the tubing. Nevertheless, the results show that the lower temperature gradient needs a slightly

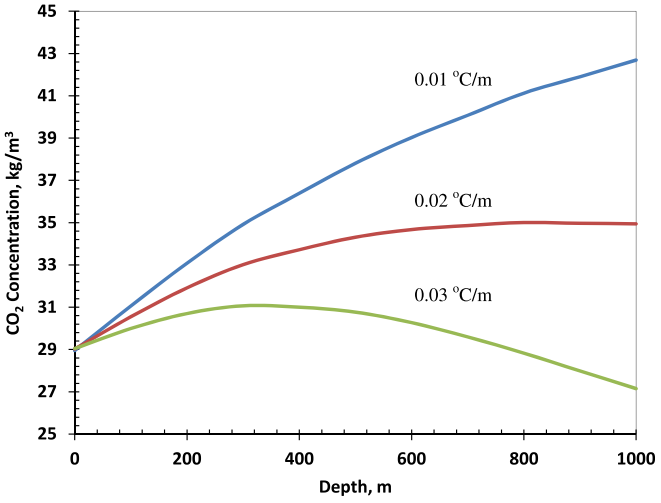

Fig. 4. Concentration profiles along the tubing, cases of 0.01, 0.02, and 0.03 °C/m.

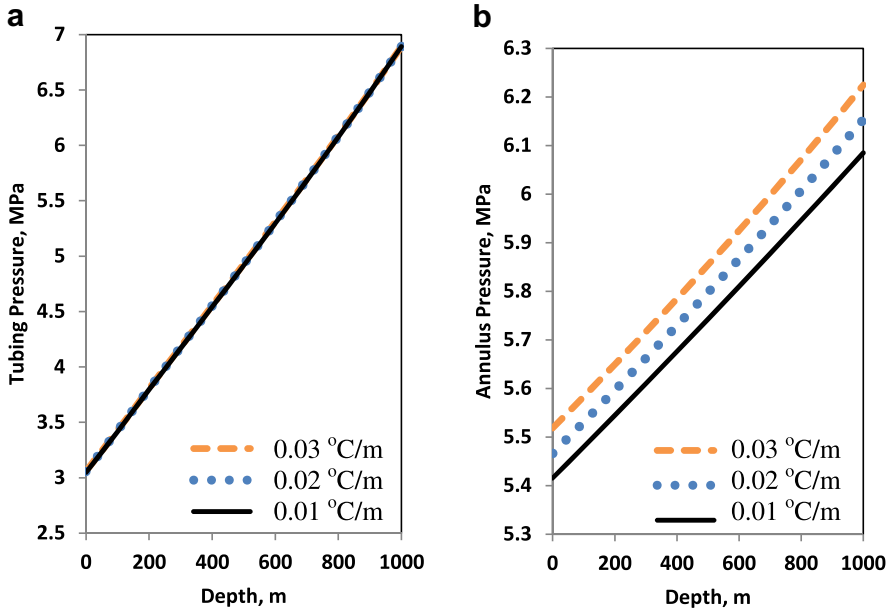

Fig. 5. Pressure profiles along the injection well for the three cases of 0.01, 0.02 and 0.03 °C/m: (a) tubing and (b) Annulus.

higher wellhead annulus pressure to achieve the same bottomhole pressure compared to the larger temperature gradient. Since the flowing temperature gradient did not affect the wellhead pressure significantly, we used a constant linear flowing temperature gradient of 0.01 °C/m in the design calculation that follows. This leads to a more conservative estimate of the required power for the pump and compressor.

The developed model was used to simulate a multi-valve injection scheme. Fig. 6 depicts a schematic diagram of the proposed injection well string configuration for injecting CO_2-brine mixtures into a saline aquifer. The injection well characteristics and operating conditions are described in this figure.

The pressure profiles along the tubing and annulus for a system with five injection valves are shown in Fig. 7. In this analysis,

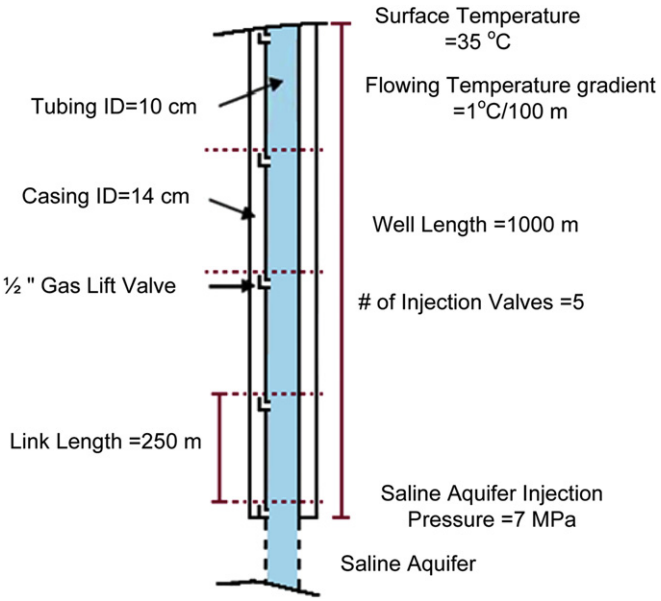

Fig. 6. Schematic of simulated injection well configuration.

30,000 kg/hr (~0.26 Mt/yr) brine and 20,000 kg/hr (~0.17 Mt/year) of CO_2 were injected. These pressure profiles show that CO_2 was pushing through first three valves. Since the upstream pressure was less than the downstream pressure at the fourth and fifth injection points, there was no injection through the last two valves. The amount of injected CO_2 for each valve is also shown in Fig. 7.

A sensitivity analysis was performed on the effect of the CO_2 injection rate into the annulus. The results shown in Table 1 reveal that when the CO_2 introduced into the casing decreased, the number of operating valves decreased. The red cells in Table 1 show those injection valves that were not operating. The mass flow rates of the injected CO_2 for the operating valves (open valves) are shown in the green cells.

One option for injecting CO_2 into a deep saline aquifer is CO_2 compression and subsequent injection into a well without brine injection, which is referred to as a conventional injection technique. The results related to the conventional injection technique are obtained by running simulations with no brine injection and in the absence of the gas-lift valves. The other option is to use the well string configuration proposed in this work. In the following paragraphs, simulations of these two approaches are described, and their results are compared.

Figs. 8 and 9 show the required wellhead injection pressures for different rates of CO_2 and brine injection using the developed design. In addition, the pressure required from a compressor station for the conventional injection technique is also shown. The results show that when the conventional injection scheme was used, the required wellhead pressure was almost constant and equal to 6.82 MPa. Simulation results reveal that when the proposed design was applied, the required compressor discharge pressure decreased.

In Fig. 8, a constant water injection rate of 0.26 Mt/yr was used. The results shown in Fig. 8 demonstrate that as the CO_2 injection rate increased, the difference in compressor discharge pressures for the two injection options reached a plateau. This plateau shows a 1 MPa pressure difference between the conventional injection scheme and the proposed model. As demonstrated in the following section, this pressure difference for the compression of CO_2 can be translated into significant energy savings. At very high flow rates of

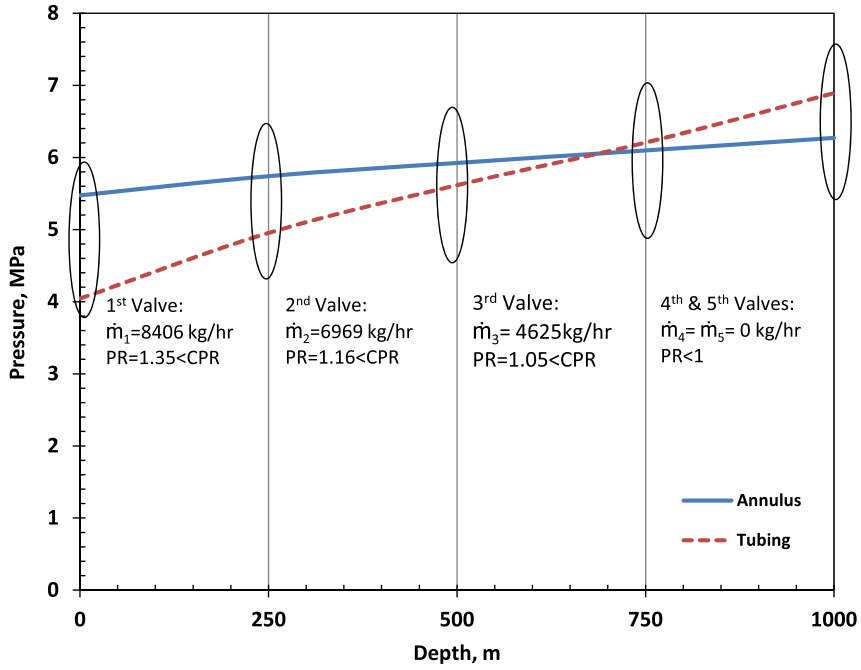

Fig. 7. Annulus and tubing pressure profiles with ½ in gas-lift valves. PR and CPR are the pressure ratio and critical pressure ratio, respectively. In this analysis, 30,000 kg/hr (~0.26 Mt/yr) brine and 20,000 kg/hr (~0.17 Mt/year) of CO_2 were injected.

Table 1
ON and OFF gas-lift valves in the system; the red cells show those injection valves that were not operating; the mass flow rates of the injected CO_2 for the operating valves (open valves) are shown in the green cells.

Injected Brine Flow Rate (kg/hr)	30,000					
Injected CO_2 Flow Rate (kg/hr)	30,000	25,000	20,000	10,000	5000	2500
Injection Point	Gas-Lift Valve Flow Rate (kg/hr)					
1	8690	8692	8406	6317	4709	2500
2	8065	7623	6969	3683	291	0
3	6835	5863	4625	0	0	0
4	4983	2822	0	0	0	0
5	1427	0	0	0	0	0

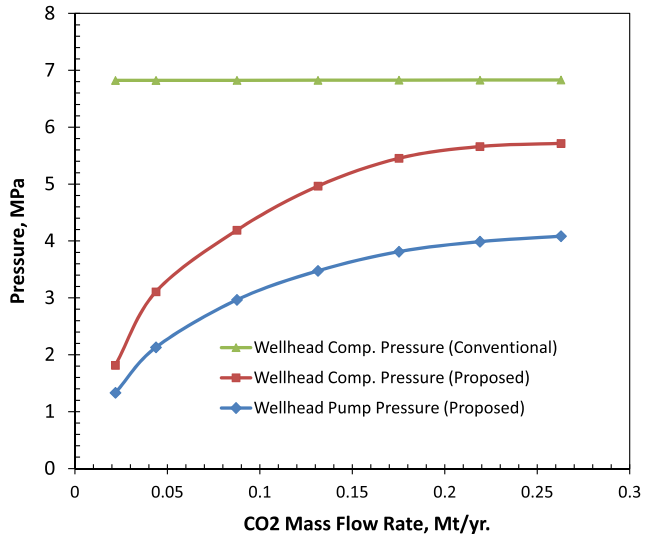

Fig. 8. Wellhead pump and compressor discharge pressures required for various injection rates of CO_2 at a constant injection rate of 0.26 Mt/yr of water.

water the liquid hold up in the tubing increases. This leads to a lower wellhead tubing pressure and consequently a greater difference between compressor discharge pressures for the two injection options. It is likely that, at very high flow rates beyond 0.26 Mt/yr of water this pressure difference increases due to larger water hold up in the tubing. This condition is more favorable in terms of energy savings as a result of lower compressor discharge pressures for the proposed scheme.

Fig. 9 depicts the required wellhead compressor and pump discharge pressures for different water injection rates and a constant CO_2 injection rate of 0.18 Mt/yr. The results show that, at higher water injection rates, the required pump and compressor discharge pressures decreased by increasing the water injection rate, as a result of an increase in the water hold up in the well tubing. This is because the static pressure gain due to liquid hold up is dominant over the frictional pressure loss.

4.2. Economics

We investigated a scenario where 1 Mt/yr of CO_2 generated from a coal-fired power plant was captured and injected into a deep saline aquifer for a period of 30 years. A coal-fired power plant operating at 33% efficiency produces ~3.79 PJ of electricity for

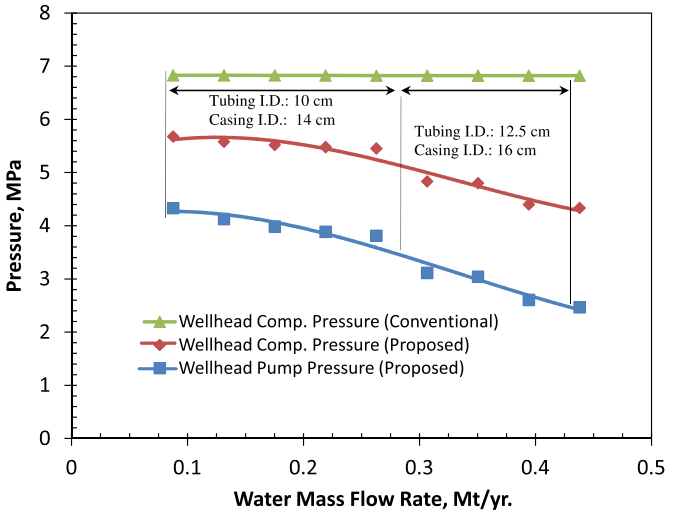

Fig. 9. Wellhead pump and compressor discharge pressures required for different injection rates of water and a constant CO_2 injection rate of 0.18 Mt/yr.

every 1 Mt of produced CO_2 per year. We assumed that the cost of drilling and well completion was an insignificant cost compared to the cost of CO_2 capture, which would be in the order of ~$1000 million (equivalent to a capture cost of 33$/t$CO_2$). We also assumed the compression of CO_2 from atmospheric pressure up to the wellhead injection pressure. We further assumed a cost for CO_2-neutral electricity of 6 c/kWhr.

To compare the energy consumption of the proposed and conventional injection techniques, total compression and pumping energy consumption for the sequestration of 1 Mt/yr of CO_2 was calculated as a percentage of energy generated in the power plant. Fig. 10 shows the total energy consumption as a percent of energy generated versus the CO_2 mass flow rate for a constant water injection rate of 0.26 Mt/yr per well (a total CO_2 sequestration of 1 Mt/yr). Fig. 11 shows the total energy consumption as a percent of energy generated versus the water mass flow rate for a constant CO_2 injection rate of 0.18 Mt/yr per well (a total CO_2 sequestration of 1 Mt/yr). The percent reduction in compression and pumping energy consumption as a result of using the proposed technique is also shown in these figures. The results show that when the

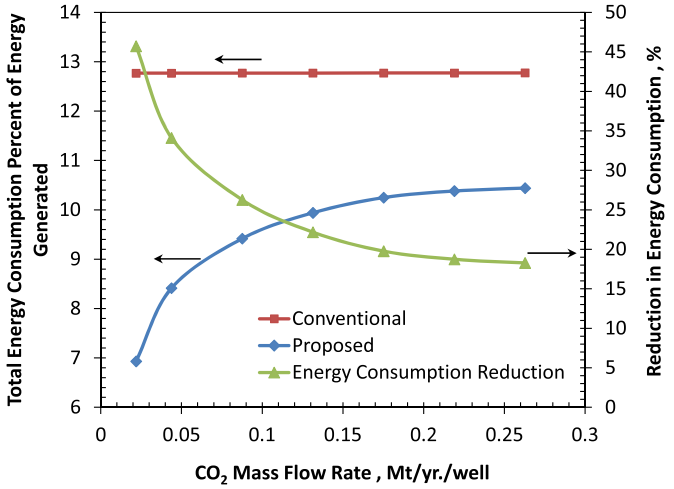

Fig. 10. Total energy consumption percent of energy generated versus CO_2 mass flow rate for a constant water injection rate of 0.26 Mt/yr per well (a total CO_2 sequestration of 1 Mt/yr). The percent reduction in compression and pumping energy consumption as a result of using the proposed technique is also shown.

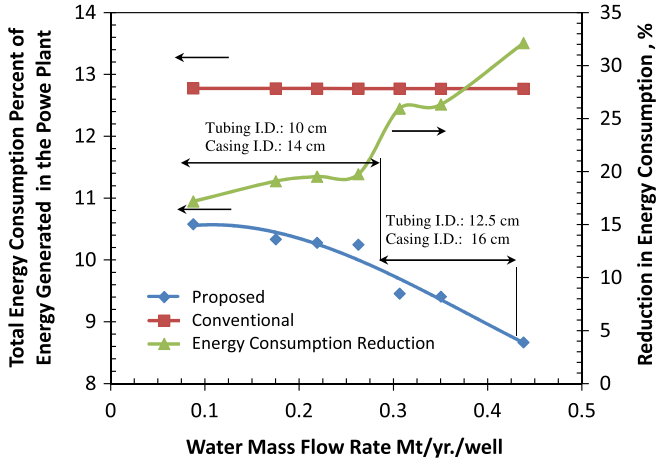

Fig. 11. Total energy consumption percent of energy generated versus water mass flow rate for a constant CO_2 injection rate of 0.18 Mt/yr per well (a total CO_2 sequestration of 1 Mt/yr). The percent reduction in compression and pumping energy consumption as a result of using the proposed technique is also shown.

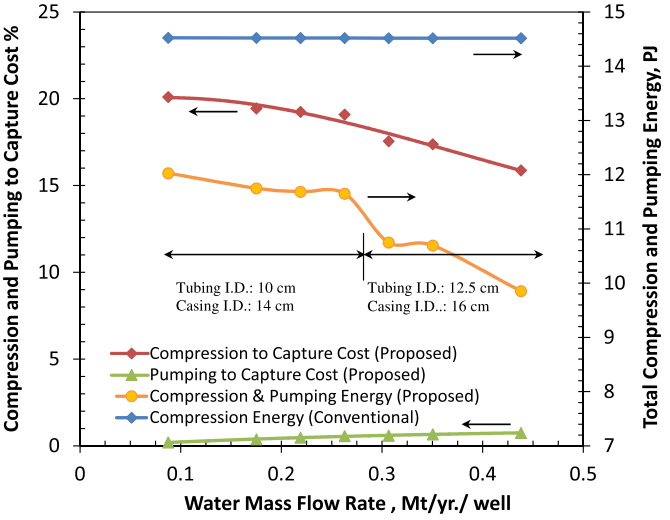

Fig. 12. Compression and pumping cost percent of CO_2 capture cost for the conventional and proposed techniques. The total compression and pumping energy for the proposed and conventional CO_2 injection schemes is also shown.

proposed design was utilized, the total energy consumed for compression and pumping decreased significantly.

A sensitivity analysis was conducted based on CO_2 injection using six injection wells with a constant injection rate of CO_2 (0.18 Mt/yr per well) and different water injection rates. Fig. 12 shows the CO_2 compression and pumping cost compared to the capture cost for a 30-year injection period. The results show that the water pumping costs were negligible compared to the CO_2 compression costs and the proposed design could potentially decrease the overall compression cost. In addition, the compression and pumping to capture costs decreased by increasing the water injection rate, which seems promising.

5. Summary and conclusions

A new downhole injection well string design has been proposed for the simultaneous injection of CO_2 and water into deep saline aquifers in this article. A model has been developed for the simulation of the concurrent injection of CO_2 and water. The proposed design has been successfully simulated for different CO_2 and water

injection flow rates; the simulation results demonstrate that the required compression cost for CO_2 injection is lower than when a conventional injection well is used for CO_2 injection. The results also show that the proposed design could potentially result in a decrease of ~33% in the total energy consumption for CO_2 compression. These results have immediate applications for field-scale implementation of CO_2 geological storage.

Acknowledgments

The authors would like to thank two reviewers for useful comments that greatly improved quality of the presentation. The financial support of the Natural Sciences and Engineering Research Council of Canada (NSERC), Institute for Sustainable Energy, Environment and Economy (ISEEE), Centre for Environmental Engineering Research and Education (CEERE), Alberta Innovates, and Foundation CMG are acknowledged.

References

[1] Intergovernmental Panel on Climate Change (IPCC). Summary for policymakers. In: Metz B, Davidson OR, Bosch PR, Dave R, Meyer LA, editors. Climate change 2007: mitigation. Contribution of working group III to the fourth assessment report of the IPCC. Cambridge, United Kingdom and New York, NY, USA: Cambridge University Press; 2007.
[2] Holloway S. Underground sequestration of carbon dioxide as a viable greenhouse gas mitigation option. Energy 2005;30:2318–33.
[3] Buttinelli M, Procesi M, Cantucci B, Quattrocchi F, Boschi E. The geo-database of caprock quality and deep saline aquifers distribution for geological storage of CO_2 in Italy. Energy 2011;36:2968–83.
[4] Intergovernmental Panel on Climate Change (IPCC) 2005. Special report on carbon dioxide capture and storage. Cambridge University Press; 2005.
[5] Gale J. Geological storage of CO_2: what do we know, where are the gaps and what more needs to be done? Energy 2004;29(9–10):1329–38.
[6] Bachu S, Adams JJ. Estimating CO_2 sequestration capacity in solution in deep saline aquifers. Energ Convers Manag 2003;44(20):3151–75.
[7] Gilfillan SMV, Sherwood Lollar B, Holland G, Blagburn G, Stevens S, Schoell M, et al. Solubility trapping in formation water as dominant CO_2 sink in natural gas fields. Nature 2009;458:614–8.
[8] Kumar A, Ozah R, Noh M, Pope GA, Bryant S, Sepehrnoori K, et al. Reservoir simulation of CO_2 storage in deep saline aquifers. Soc Pet Eng J 2003;10(3):336–48.
[9] Flett M, Gurton R, Weir GJ. Heterogeneous saline formations for carbon dioxide disposal: Impact of varying heterogeneity on containment and trapping. J Pet Sci Eng 2007;57:106–18.
[10] Juanes R, Spiteri EJ, Orr Jr FM, Blunt MJ. Impact of relative permeability hysteresis on geological CO_2 storage. Adv Water Resour 2006;42:W12418.
[11] Bachu S, Gunter WD, Perkins EH. Aquifer disposal of CO_2: hydrodynamic and mineral trapping. Energ Convers Manag 1994;35:269–79.
[12] Pruess K, Xu T, Apps J, García J. Numerical modeling of aquifer disposal of CO_2. Soc Pet Eng J 2003:49–60.
[13] Labus K, Bujok P. CO_2 mineral sequestration mechanisms and capacity of saline aquifers of the Upper Silesian Coal Basin (Central Europe)–modeling and experimental. Energy 2011;36:4974–82.
[14] van der Meer LGH. The conditions limiting CO_2 storage in aquifers. Energy Convers Manag 1993;34(9–11):959–66.
[15] Ghaderi A, Keith D, Leonenko Y. Feasibility of injecting large volumes of CO_2 into aquifers. In: Proc. GHGT-9 2009. Washington, DC, USA; Nov 16–20.
[16] Holloway S, Pearce JM, Hards VL, Oshumi T, Gayle J. Natural emissions of CO_2 from the geosphere and their bearing on the geological storage of carbon dioxide. Energy 2007;32:1201–994.
[17] Hassanzadeh H, Pooladi-Darvish M, Keith D. Accelerating CO_2 dissolution in saline aquifers for geological storage - Mechanistic and sensitivity studies. Energy Fuels 2009;23(6):3328–36. http://dx.doi.org/10.1021/ef900125m.
[18] Keith D, Hassanzadeh H, Pooladi-Darvish M. Reservoir engineering to accelerate dissolution of stored CO_2 in brines. Proceedings of 7th International Conference on greenhouse gas control Technologies 2004. Cheltenham, UK: IEA Greenhouse Gas Program; 2005.
[19] Hassanzadeh H, Pooladi-Darvish M, Keith D. Accelerating CO_2 dissolution in saline aquifers for geological storage–mechanistic and sensitivity studies. Energ Fuel 2009;23(6):3328–36.
[20] Burton M, Bryant S. Surface dissolution: minimizing groundwater impact and leakage risk simultaneously. GHGT-9, 9th International Conference on greenhouse gas control Technologies (November 16–20, 2008; Washington, DC). Energy Procedia 2009;1:3707–14.
[21] Zendehboudi S, Khan A, Carlisle S, Leonenko Y. Ex situ dissolution of CO_2: a new engineering methodology based on mass-transfer perspective for enhancement of CO_2 sequestration. Energ Fuel 2011;25(7):3323–33.
[22] Guo B, Lyons WB, Ghalambor A. Petroleum production engineering: a computer assisted approach. Elsevier; 2007.
[23] Guo B, Ghalambor A. Natural gas engineering Handbook. Houston, TX: Gulf Publishing Company; 2005.
[24] Alves IN, Alhanati FJS, Shoham O. A unified model for predicting flowing temperature distribution in wellbores and pipelines. SPE Prod Eng J 1992; 7(4):363–7.
[25] Hassanzadeh H, Pooladi-Darvish M, Elsharkawy AM, Keith D, Leonenko Y. Predicting PVT data for CO_2-brine mixtures for black-oil simulation of CO_2 geological storage. Int J Greenh Gas Con 2008;2(1):65–77.
[26] Beggs HD, Brill JP. A study of two-phase flow in inclined pipes. J Petr Tech 1973:607–13.
[27] Roberson JA, Crowe CT. Engineering fluid mechanics. New York: J. Wiley & Sons; 1997.
[28] Chen JJ. A simple explicit formula for the estimation of pipe friction factor. Proc Inst Civ Eng 1984;77(2):49–55.
[29] Martin D, Peters G. The application of Newton's method to network analysis by digital computer. J Inst Water Eng 1963;17:115.